Wavepacket scattering of Dirac and Schrödinger particles on potential and magnetic barriers

J. Phys.: Condens. Matter **23** (2011) 275801 (16pp) doi:10.1088/0953-8984/23/27/275801

Wavepacket scattering of Dirac and Schrödinger particles on potential and magnetic barriers

Kh Yu Rakhimov[1,2,3], **Andrey Chaves**[1,4], **G A Farias**[4] **and F M Peeters**[1,4]

[1] Department of Physics, University of Antwerp, Groenenborgerlaan 171, B-2020 Antwerp, Belgium
[2] Physics Department, National University of Uzbekistan, 700174 Tashkent, Uzbekistan
[3] Turin Polytechnic University in Tashkent, 700174 Tashkent, Uzbekistan
[4] Departamento de Física, Universidade Federal do Ceará, Caixa Postal 6030, Campus do Pici, 60455-900 Fortaleza, Ceará, Brazil

E-mail: andrey@fisica.ufc.br and francois.peeters@ua.ac.be

Received 7 April 2011, in final form 19 May 2011
Published 17 June 2011
Online at stacks.iop.org/JPhysCM/23/275801

Abstract
We investigate the dynamics of a charged particle moving in a graphene layer and in a two-dimensional electron gas, where it obeys the Dirac and the Schrödinger equations, respectively. The charge carriers are described as Gaussian wavepackets. The dynamics of the wavepackets is studied numerically by solving both quantum-mechanical and relativistic equations of motion. The scattering of such wavepackets by step-like magnetic and potential barriers is analysed for different values of wavepacket energy and width. We find: (1) that the average position of the wavepacket does not coincide with the classical trajectory, and (2) that, for slanted incidence, the path of the centre of mass of the wavepacket does not have to penetrate the barrier during the scattering process. Trembling motion of the charged particle in graphene is observed in the absence of an external magnetic field and can be enhanced by a substrate-induced mass term.

(Some figures in this article are in colour only in the electronic version)

1. Introduction

The scattering of classical, quantum and relativistic particles is fundamentally different from each other. The tunnelling effect, which allows quantum particles to penetrate classically forbidden regions of higher potential, is essentially a quantum mechanical phenomenon, i.e. it cannot be described in terms of Newtonian mechanics. This fascinating effect constitutes the fundamental paradigm in the development of the widely used resonance tunnelling diodes [1]. The dynamics of a wavepacket obeying the Schrödinger equation provides a powerful tool to investigate scattering problems of quantum particles, which has been used to model, for example, the lifetime of a quasi-bound electron on the surface of liquid helium [2], the exciton escape in semiconductor quantum dots with finite barriers [3] and the Aharonov–Bohm interference in semiconductor quantum rings [4].

The propagation of wavepackets has also been investigated recently in an ideal graphene monolayer [5, 6], a material which received a revival of interest after the pioneering paper by Geim *et al* [7]. It has been demonstrated that low-energy electrons in graphene obey the Dirac equation for massless fermions [8]. Thus, the experimental isolation of graphene layers was undoubtedly a very important scientific achievement, since it opened the possibility of using electrons in graphene to simulate effects which were supposed to be observed only for relativistic particles.

It is known that relativistic particles show qualitatively new and unexpected dynamic features [9–11]. An example is the trembling motion of relativistic electrons (also called zitterbewegung [12]), caused by the interference between positive and negative energy states forming the electron wavepacket [13]. Such an interference was theoretically investigated by Thaller [9], who applied the Dirac equation

to study the dynamics of a relativistic one-dimensional wavepacket and reported not only on the zitterbewegung, but also on different interesting phenomena coming from this interaction, e.g. the superluminal propagation of the wavepackets maxima. Trembling motion of 3D electron wavepackets was also under intensive research (see, e.g., [11]) after its prediction by Ferrari and Russo [14]. Very recently, Demikhovskii *et al* [10] studied the relativistic dynamics of 3D Gaussian electron wavepackets with different spin polarizations solving the Dirac equation both analytically and numerically. They showed that the direction of both average electron velocity and trembling motion can be predicted by analysing the symmetry properties of the solutions of the massless Dirac equation. Although the first prediction of zitterbewegung dates from almost 80 years ago [12], the first experimental observation of this effect was reported only very recently by Gerritsma *et al* [15], where such a trembling motion was observed in a system of trapped ions, which simulates a $(1 + 1)$-dimensional Dirac equation. Nevertheless, zitterbewegung of quasi-relativistic electrons in graphene is yet to be observed experimentally, which has led to several theoretical works suggesting different possibilities of observing this effect. For instance, in a recent paper, Rusin and Zawadzki [16] studied the effect of an external magnetic field on the trembling motion of a wavepacket generated by a laser pulse. The effect of the magnetic field on the zitterbewegung was found to be considerable and observable in an experiment [17]. Maksimova *et al* [5] showed that the time dependence of the shape of the electron wavepacket in graphene depends on the correlation between the initial states of the parts of the electron wavefunction belonging to the sub-lattices A and B, which is represented by a pseudo-spinor. Depending on the pseudo-spin polarization, the motion of the centre of the wavepacket, experiencing the zitterbewegung with a transient character, may even occur in the direction perpendicular to the average momentum, along with splitting of the initial wavepacket into two parts with opposite velocities.

Another example of the unique features of the dynamics of Dirac particles is the so-called Klein tunnelling: when a massless Dirac particle reaches a potential barrier with normal incidence, it is fully transmitted through the barrier as a hole state [18]. In the past, attempts to experimentally detect this effect have faced difficulties due to the high fields required to observe this effect with relativistic particles. However, the discovery of graphene brought about the possibility of observing quasi-relativistic physics in the laboratory, which made possible the experimental observation of Klein tunnelling, inferred by the high conductance observed in the presence of a gate voltage in graphene, which implies a high transmission probability through the gate-induced barrier potential [19, 20]. On the other hand, this effect might also be considered as an obstacle in the development of novel graphene-based quantum well and quantum dot devices, since the gate-induced electrostatic potentials are not able to confine electrons [21].

The scattering of Schrödinger and Dirac particles by magnetic barriers has also been the subject of recent studies. The former was investigated by Matulis *et al* [22] and models the situation where an electron in a semiconductor passes from a region where the magnetic field is screened by a superconducting covering layer to a region without the superconducting cover, where it experiences the external field. The latter was studied in [23–25], modelling the same situation, but for electrons in a graphene monolayer, instead of a semiconductor. Magnetic barriers for Dirac particles can also be obtained by specific forms of strain in graphene, as reported in subsequent papers [26].

In this work, we propose a numerical method for solving the time-dependent Schrödinger and Dirac equations, based on the split-operator technique [4]. We use this method to study the propagation of a Gaussian wavepacket representing electrons in a two-dimensional electron gas (2DEG) and in graphene. The scattering of such wavepackets by step-like electrostatic or magnetic field barriers is analysed for different energies and widths of the packets. We demonstrate how the quantum tunnelling and the Klein tunnelling effects, for Schrödinger and Dirac particles, respectively, apply to the case where we consider a wavepacket, instead of the commonly used plane waves. We observe the trembling motion of the electrons in graphene, due to the zitterbewegung, which is converted to circle-like motion in the presence of a magnetic barrier due to the Lorentz force. Furthermore, we demonstrate how a mass term in the Dirac Hamiltonian, which can be experimentally realized by laying the graphene sheet on specific substrates [27, 28], affects the zitterbewegung of the low-energy electrons in graphene. We contrast these results with the ones obtained for an electron in a 2DEG, where the motion of nonrelativistic charge carriers is described by the quantum mechanical Schrödinger equation.

This paper is organized as follows: in section 2, we first describe the theoretical approach, which we use to study the time evolution of wavepackets in a 2DEG. Then, we use this approach to investigate the scattering problem of electrons from potential and magnetic barriers, i.e. in the presence of non-homogeneous scalar and vector fields. Section 3 starts with the description of the numerical method for the wavepacket dynamics in graphene, which we then apply to study wavepacket scattering by a mass barrier, where its influence on the zitterbewegung is discussed, as well as by potential and magnetic barriers, where we discuss about the Klein tunnelling and the effect of the Lorentz force on the trajectories, respectively. All our findings are summarized in section 4.

2. Time evolution of wavepackets in a 2DEG

Consider a particle described by the wavefunction $\Psi(x, y, t)$, whose dynamics is determined by the Hamiltonian H. The time evolution of such a particle by a time step Δt is given by applying the time-evolution operator on the initial wavefunction, so that

$$\Psi(x, y, t + \Delta t) = \exp\left(-\frac{\mathrm{i}}{\hbar} H \Delta t\right) \Psi(x, y, t). \qquad (1)$$

Usually, the exponential of an operator cannot be performed exactly. On the other hand, many approximations for the exponential in equation (1) were proposed by previous works, for instance, the split-operator technique [29], which combines the separation between kinetic and potential terms in the Hamiltonian [30] with the Cayley form [31] of the exponential in the time-evolution operator. This technique, which has been applied successfully in the study of wavepackets in semiconductors [4] and graphene [32], is used in this work and can be easily implemented computationally.

The main idea of the split-operator technique is to separate terms which depend on the real and reciprocal space coordinates. Let us first consider the dynamics of a wavepacket confined in the x–y plane and obeying the Schrödinger equation with the Hamiltonian

$$H_{\mathrm{S}} = \frac{\vec{p}^2}{2m} + V(x, y), \tag{2}$$

where $V(x, y)$ is an external potential. Such a Hamiltonian is found, for example, in the effective mass approximation for semiconductors, where the electron mass assumes a value different from the free-electron mass m_0. Following the split-operator technique for this case, the time-evolution operator in equation (1) becomes

$$\mathrm{e}^{-\frac{\mathrm{i}}{\hbar}H\Delta t} = \mathrm{e}^{-\frac{\mathrm{i}\Delta t}{2\hbar}V}\mathrm{e}^{-\frac{\mathrm{i}\Delta t}{\hbar}\frac{\vec{p}^2}{2m}}\mathrm{e}^{-\frac{\mathrm{i}\Delta t}{2\hbar}V} + \mathrm{O}(\Delta t^3), \tag{3}$$

where the $\mathrm{O}(\Delta t^3)$ term is a consequence of the non-commutativity between the kinetic and potential terms. In order to apply the exponential of the kinetic term, we split this exponential as

$$\exp\left(-\frac{\mathrm{i}\Delta t}{\hbar}\frac{\vec{p}^2}{2m}\right) = \exp\left(-\frac{\mathrm{i}\Delta t}{\hbar}\frac{p_x^2}{2m}\right)\exp\left(-\frac{\mathrm{i}\Delta t}{\hbar}\frac{p_y^2}{2m}\right), \tag{4}$$

and use the Cayley form for each term:

$$\exp\left(-\frac{\mathrm{i}\Delta t}{\hbar}\frac{p_j^2}{2m}\right) = \frac{1 - \frac{\mathrm{i}\Delta t}{2\hbar}\frac{p_j^2}{2m}}{1 + \frac{\mathrm{i}\Delta t}{2\hbar}\frac{p_j^2}{2m}} + \mathrm{O}(\Delta t^2). \tag{5}$$

Since the momenta p_x and p_y commute, the splitting in equation (4) produces no additional error. The partial differential operators in p_x and p_y are written in discrete form by using the finite difference scheme. In the presence of an applied magnetic field $\vec{B} = \vec{\nabla} \times \vec{A}$, we use the gauge-independent form of the discretized momentum operators, where the vector potential $\vec{A}$ is accounted for as a phase shift between the grid points, similar to the Peierls phase in tight-binding models [33]. Applying the formalism described above to equation (1), one finally obtains the time evolution of a Schrödinger wavepacket as

$$\Psi(x, y, t + \Delta t) \approx \mathrm{e}^{-\frac{\mathrm{i}\Delta t}{2\hbar}V}\mathrm{e}^{-\frac{\mathrm{i}\Delta t}{\hbar}\frac{p_x^2}{2m}}\mathrm{e}^{-\frac{\mathrm{i}\Delta t}{\hbar}\frac{p_y^2}{2m}}\mathrm{e}^{-\frac{\mathrm{i}\Delta t}{2\hbar}V}\Psi(x, y, t), \tag{6}$$

where the multiplications are made step by step:

$$\xi(x, y, t) = \exp\left(-\frac{\mathrm{i}\Delta t}{2\hbar}V\right)\Psi(x, y, t) \tag{7a}$$

$$\left(1 + \frac{\mathrm{i}\Delta t}{2\hbar}\frac{p_y^2}{2m}\right)\eta_y(x, y, t) \approx \left(1 - \frac{\mathrm{i}\Delta t}{2\hbar}\frac{p_y^2}{2m}\right)\xi(x, y, t) \tag{7b}$$

$$\left(1 + \frac{\mathrm{i}\Delta t}{2\hbar}\frac{p_x^2}{2m}\right)\eta_x(x, y, t) \approx \left(1 - \frac{\mathrm{i}\Delta t}{2\hbar}\frac{p_x^2}{2m}\right)\eta_y(x, y, t) \tag{7c}$$

$$\Psi(x, y, t + \Delta t) \approx \exp\left(-\frac{\mathrm{i}\Delta t}{2\hbar}V\right)\eta_x(x, y, t), \tag{7d}$$

i.e., we first obtain the auxiliary function $\xi(x, y, t)$ from equation (7*a*), which is then used to calculate $\eta_y(x, y, t)$ in equation (7*b*). Using the auxiliary function $\eta_y(x, y, t)$ in equation (7*c*), we obtain a new auxiliary function $\eta_x(x, y, t)$, which is finally used in equation (7*d*) to obtain the propagated wavepacket $\Psi(x, y, t + \Delta t)$. The $\mathrm{O}(\Delta t^2)$ and $\mathrm{O}(\Delta t^3)$ terms are dropped by assuming a small time step Δt. Thus, the split-operator technique for Schrödinger particles described above is accurate up to second order in time.

Equations (4)–(7*d*) clarify the advantage of using the split-operator technique: if one makes no separation between kinetic and potential terms, as in equation (3), one would have to make the Cayley form in equation (5) for the full Hamiltonian H, instead of the momentum in a single direction, p_j. Eventually, we must use a finite difference scheme and write equation (5) in a matrix form, and the matrix representation of the full Hamiltonian, in the bi-dimensional case, consists of a five-diagonal matrix, which is much harder to handle than the tridiagonal matrix representing p_j. So, the split-operator technique provides a way to break the operations with the full Hamiltonian by a series of operations with simpler tridiagonal matrices, by the price of considering a small value for Δt, due to the non-commutativity of the operators involved.

As the initial wavefunction, we choose a symmetric Gaussian function of the form

$$\Psi(x, y) = \frac{1}{d\sqrt{2\pi}}\exp\left[-\frac{(x - x_0)^2}{2d^2} - \frac{(y - y_0)^2}{2d^2} + \mathrm{i}\overrightarrow{k^{(0)}} \cdot \vec{r}\right], \tag{8}$$

where d is the width of the wavepacket. For a parabolic energy–momentum relation, the wavevector $\overrightarrow{k^{(0)}}$ is related to the energy as $k^{(0)} = |\overrightarrow{k^{(0)}}| = \sqrt{2mE/\hbar^2}$, and $k_x^{(0)} = k^{(0)}\sin\varphi$ and $k_y^{(0)} = k^{(0)}\cos\varphi$, where φ is the angle of propagation. The Fourier transform of the wavefunction equation (8) is

$$\tilde{\Psi}(k_x, k_y) = \frac{1}{(2\pi)^2}\exp\Bigg[-\mathrm{i}(k_x - k_x^{(0)})x_0 - \frac{(k_x - k_x^{(0)})^2 d^2}{2} - \mathrm{i}(k_y - k_y^{(0)})y_0 - \frac{(k_y - k_y^{(0)})^2 d^2}{2}\Bigg], \tag{9}$$

which is a Gaussian function in reciprocal space, centred at $\vec{k}^0$ and with width d^{-1}. Thus, the wavepacket equation (8) represents a Gaussian distribution not only for the particle position in real space, but also for the particle momentum.

In the following we will calculate the centre-of-mass coordinates of the wavepacket $\langle\vec{r}\rangle = (\langle x\rangle, \langle y\rangle)$ and its velocity $\vec{v} = (v_x, v_y)$ as

$$v_x = \frac{\mathrm{d}\langle x\rangle}{\mathrm{d}t}, \qquad v_y = \frac{\mathrm{d}\langle y\rangle}{\mathrm{d}t}, \tag{10}$$

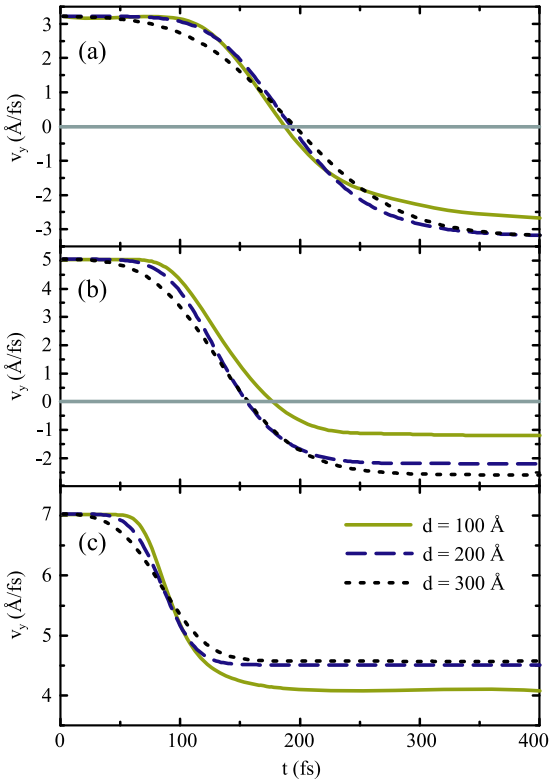

Figure 1. Electron velocity as a function of time in the presence of a step barrier potential of height $V_0 = 50$ meV. We consider initial wavepackets with $\varphi = 0$ and different energies (a) $E = 20$ meV, (b) $E = 50$ meV and (c) $E = 100$ meV, and three different widths d.

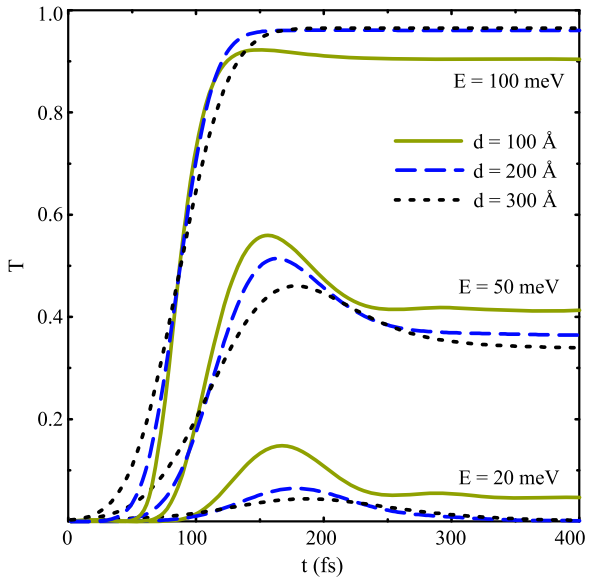

Figure 2. Probabilities to find the particle inside the barrier of height $V_0 = 50$ meV as a function of time.

with $\langle x\rangle = \langle\Psi|x|\Psi\rangle$ and $\langle y\rangle = \langle\Psi|y|\Psi\rangle$. These quantities will be useful for the study of the wavepacket trajectories in the following sub-sections.

2.1. Scattering by a potential barrier

Let us study the scattering of the wavepacket equation (8) by a potential step which is constant in the x direction, defined as $V(y) = V_0\Theta(y)$, where $\Theta(y)$ is the Heaviside step function.

In the case of normal incidence, a classical particle with velocity $\vec{v}^{\,\mathrm{i}} = (0, v_y)$ in such a system is reflected by the barrier at $y = 0$ and returns with final velocity $\vec{v}^{\,\mathrm{f}} = (0, -v_y)$ if the particle energy is $E < V_0$, otherwise (i.e. for $E > V_0$) it is transmitted with lower velocity. On the other hand, a quantum particle described by a plane wave with energy $E < V_0$ can still penetrate the barrier region and has a finite probability of reflection even when $E > V_0$. Hence, in the case of a Gaussian wavepacket, one expects results which are quite different from the classical picture: since the wavepacket is composed of a linear superposition of plane waves with different energies, part of the packet which has energy lower than V_0 must be reflected, whereas the part with energy larger than V_0 has a finite probability to be transmitted, so that the average velocity after scattering is given by a combination of positive and negative velocities.

As an example, figure 1 shows the velocity as a function of time for a wavepacket describing an electron in a GaAs 2DEG, with effective mass $m = 0.067m_0$, in the presence of a potential step barrier $V_0 = 50$ meV, moving head on towards the barrier for different initial energies $E = 20$ (a), 50 (b) and 100 meV (c), for various wavepacket sizes $d = 100$, 200 and 300 Å. The probability of finding the wavepacket inside the barrier is calculated as $T = \int_{-\infty}^{\infty} \mathrm{d}x \int_{0}^{\infty} \mathrm{d}y\, |\Psi|^2$, which is shown in figure 2 as a function of time. For $t \to \infty$ this corresponds to the transmission probability. The wavepacket propagates in the direction $\varphi = 0$, i.e. $\vec{k}^{(0)} = k_y^{(0)}\hat{y}$, and is initially centred at $x_0 = -600$ Å and $y_0 = 0$. The contour plots of the squared modulus of the wavefunction (probability density) at different time steps shown in figure 3 help to visualize the wavepacket scattering by the potential step barrier. For $E = 20$ meV ($<V_0$), the transmission probability as a function of time exhibits a peak (see figure 2), due to a very short penetration inside the barrier region, which can be verified in the contour plots of the probability density in figure 3. After this peak, T decays to $T \approx 0$ for $d = 200$ and 300 Å, which means that most of the packet is reflected, leading to a final velocity $v_y^{\mathrm{f}} \approx -v_y^{\mathrm{i}}$, in accordance with the classical result. However, for $d = 100$ Å, T converges to a finite number, i.e. part of the packet is transmitted, leading to a final velocity $|v_y^{\mathrm{f}}| < |v_y^{\mathrm{i}}|$. The reason is that for smaller d the wavepacket contains a larger distribution of energies, so that the tail of the wavepacket in equation (9) with energy larger than V_0 can be transmitted, contributing to a smaller final velocity.

For average energy $E = 50$ meV ($=V_0$), as the energy distribution is symmetric around E, one would expect that less than half of the packet is transmitted, since $T < 1$ for electron energies immediately above V_0. Therefore, the final velocity is $|v_y^{\mathrm{f}}| < |v_y^{\mathrm{i}}/2|$, as observed in figure 1(b). Notice that T and, consequently, v_y^{f} for $t \to \infty$ depends on the width of the wavepacket and that T decreases with increasing d, which is reasonable, since an enlargement of the width of the packet corresponds to a narrowing of the momentum distribution, so

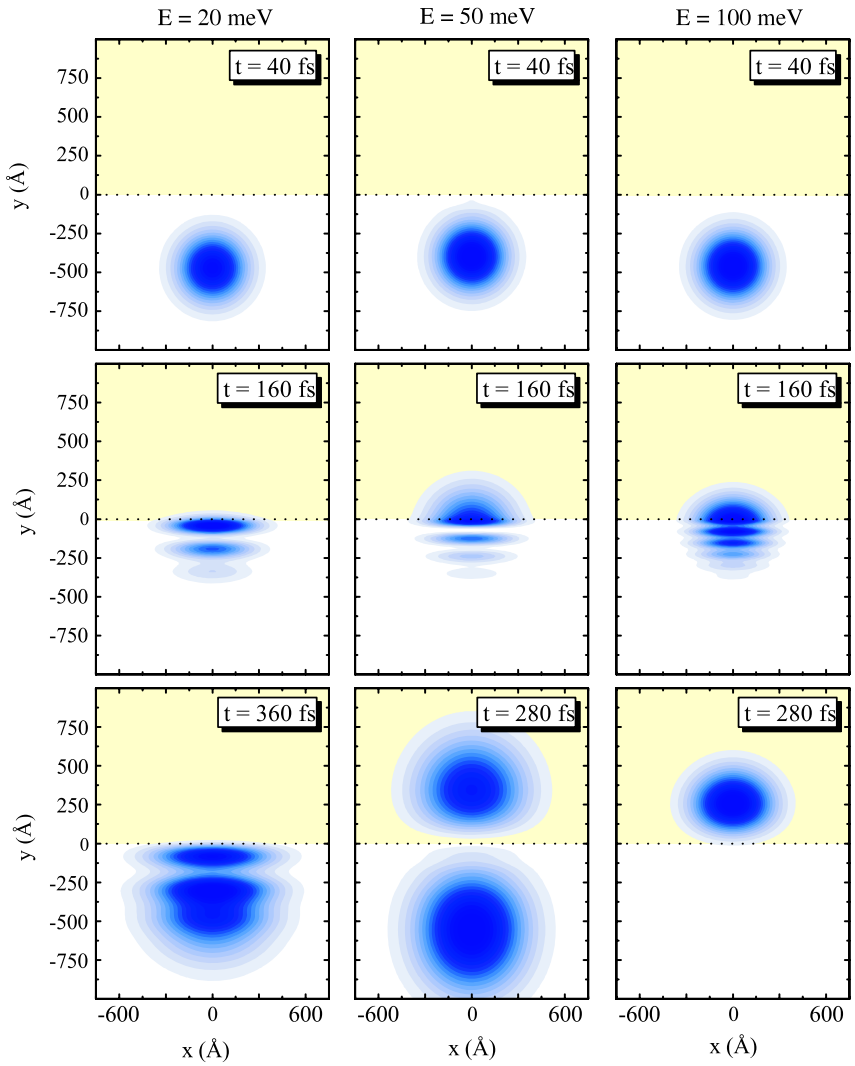

Figure 3. Contour plots of the squared modulus of the wavefunctions (probability densities) for an electron, described by a Gaussian wavefunction with width $d = 200$ Å and different values of average energy E, scattered by a step barrier potential, where the shaded area represents the $V_0 = 50$ meV region. Darker (lighter) colours represent higher (lower) values of the probability density.

that a smaller part of the packet would have energy above V_0 for larger d.

For $E = 100$ meV, less reflection is expected and the final velocity is positive due to the large transmission. Indeed, figure 2 for this energy shows final transmission probabilities close to (but lower than) 1, and the contour plots of the probability density in figure 3(c) show almost no reflection for this case. Even so, one still observes a small reflection in figure 2 for this energy, which is more pronounced for $d = 100$ Å. Notice that the d dependence is opposite from the previous two cases. Increasing d, for large time, T increases and converges to a number lower than 1 and, consequently, the final velocity converges to $v_y^{\mathrm{f}} < v_y^{\mathrm{i}}$. This indicates that, even with a narrow energy distribution, the wavepacket with energy $E = 100$ meV ($> V_0 = 50$ meV) is still not fully transmitted. In fact, the transmission probability for a plane wave scattered by a quantum step barrier with $E = 100$ meV and $V_0 = 50$ meV is $T = 4[\sqrt{E(E-V_0)}/(\sqrt{E}+\sqrt{E-V_0})^2] \approx 0.971$. Thus, even if the average energy of the wavepacket is $E > V_0$, it may contain energies below the barrier height and, as a consequence, this part of the wavepacket would be reflected; otherwise, if there is no part below V_0, the electron still has a finite probability of being reflected, just because of the quantum reflection due to the step potential discontinuity.

The non-conservation of the modulus of the velocity results partially from the fact that our wavepacket is split by the step potential, so that part is transmitted and part is reflected, exhibiting opposite signs of velocity. Naively, one may argue that we should deal with this problem as if we had two different particles, so that we can calculate the velocities of the transmitted and reflected particles by taking the derivative of their positions in the y direction, respectively given by

$$\langle y\rangle_r = \frac{\int_{-\infty}^{\infty} \mathrm{d}x \int_{-\infty}^{0} \mathrm{d}y\, \Psi^\dagger y \Psi}{\int_{-\infty}^{\infty} \mathrm{d}x \int_{-\infty}^{0} \mathrm{d}y\, |\Psi|^2} \qquad (11a)$$

$$\langle y\rangle_t = \frac{\int_{-\infty}^{\infty} \mathrm{d}x \int_{0}^{\infty} \mathrm{d}y\, \Psi^\dagger y \Psi}{\int_{-\infty}^{\infty} \mathrm{d}x \int_{0}^{\infty} \mathrm{d}y\, |\Psi|^2}, \qquad (11b)$$

with respect to time. However, the sum of the velocities of the transmitted and reflected parts calculated in this way is still not equal to the initial velocity, since

$$v_y = \frac{\partial\langle y\rangle}{\partial t} = \frac{\partial}{\partial t}\frac{\int_{-\infty}^{\infty}\mathrm{d}x\int_{-\infty}^{0}\mathrm{d}y\,\Psi^{\dagger}y\Psi}{\int_{-\infty}^{\infty}\mathrm{d}x\int_{-\infty}^{\infty}\mathrm{d}y\,|\Psi|^2} + \frac{\partial}{\partial t}\frac{\int_{-\infty}^{\infty}\mathrm{d}x\int_{0}^{\infty}\mathrm{d}y\,\Psi^{\dagger}y\Psi}{\int_{-\infty}^{\infty}\mathrm{d}x\int_{-\infty}^{\infty}\mathrm{d}y\,|\Psi|^2}, \tag{12}$$

which has a different denominator as compared to $\partial\langle y\rangle_r/\partial t + \partial\langle y\rangle_t/\partial t$. Indeed, we have only one wavepacket, and any physical property of the system should be consistent with the single-wavepacket point of view.

2.2. Scattering by a magnetic barrier

We now investigate the time evolution of the wavepacket studied in section 2.1 for $V_0 \equiv 0$, but in the presence of a magnetic step barrier, given by $\vec{B} = B_0\Theta(y)\hat{z}$. The scattering problem for such an inhomogeneous vector field is very different from the previous case [22, 25, 34]. A classical (charged) particle in such a system is expected to perform a circular trajectory with radius $R_c = \hbar k^{(0)}/eB_0$ for $y > 0$, due to the Lorentz force.

The trajectory performed by the centroid of the wavepacket, i.e. by $\langle\vec{r}\rangle$, in the x–y plane is shown by the solid curves in figure 4, where we clearly observe circular- and semicircular-like trajectories for $y > 0$. Circles fitted to the numerical results are shown by the dashed curves. Even so, these circles differ from those obtained from the classical treatment of the problem: in figure 4(c), for example, the fitting gives a circle with radius $R = 504$ Å, whereas the classical path should be a circle with radius $R = 548$ Å. Alternatively, we can plot the position of the maximum of the wavepacket. This is illustrated by the symbols in figure 4, where the discrepancy with the classical path is still observed. As the wavepacket is reflected, several peaks are observed as a consequence of interference, which is the reason for the irregular trajectory.

The Ehrenfest theorem, which relates $\langle\vec{v}\rangle$ to $\langle[\vec{r}, H]\rangle$ in a way that is very similar to Liouville's theorem from Hamiltonian mechanics, is commonly interpreted as a connection between the quantum and classical mechanics. This theorem suggests that the trajectory performed by $\langle\vec{r}\rangle$ in the x–y plane in the quantum case is comparable to the one performed by a classical particle in an analogous classical problem. The reason for the partial breakdown of Ehrenfest's theorem in our results comes from the fact that, as we have a distribution of momentum states in the wavepacket, the part of the packet which has higher momentum reaches the magnetic barrier region first and performs a circle with larger radius, since the radius R_c is proportional to the momentum. When the remaining (slower) parts of the packet reach the barrier, its upper (faster) part is already travelling back, after performing the circular trajectory due to the Lorentz force. This explains the difference between the trajectories performed by classical particles and by $\langle\vec{r}\rangle$.

In figure 5(a), we observe that, as the magnetic field increases, the centre of mass of the wavepacket penetrates less

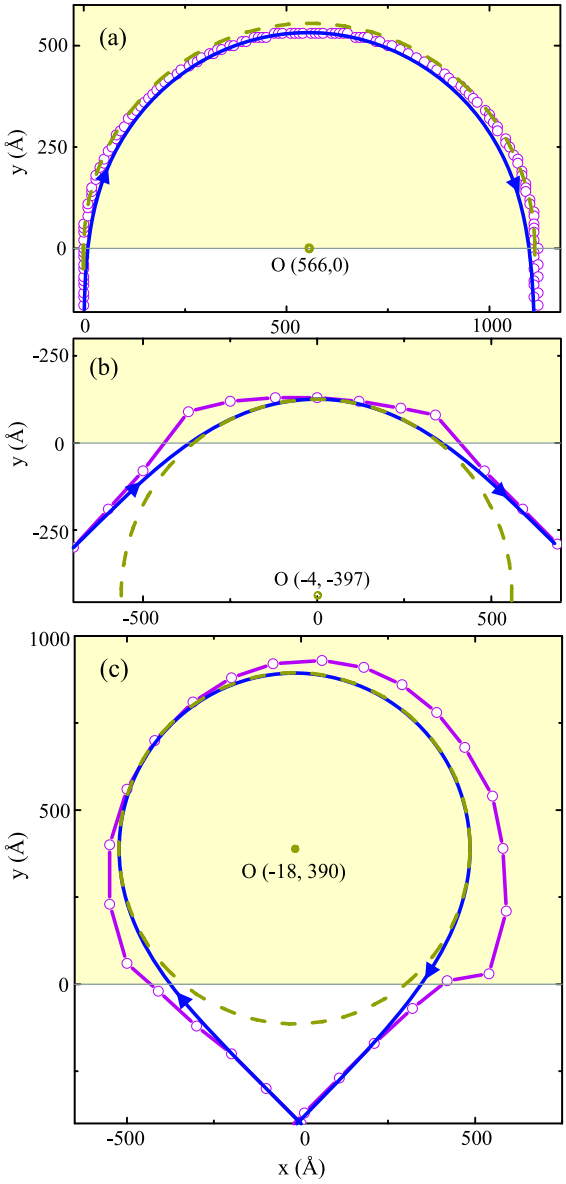

Figure 4. Trajectory of the electron wavepacket with parameters $d = 200$ Å and $E = 100$ meV, scattered by a magnetic step barrier of height $B_0 = 5$ T, represented by the shaded area. The blue solid curves are the results obtained from $\langle\vec{r}\rangle$. A few points obtained from the trajectory performed by the position of the maximum of the wavepacket are plotted as red open symbols, for comparison. We consider different incidence angles: (a) $\varphi = 0$, (b) $\varphi = \pi/4$ and (c) $\varphi = -\pi/4$. The arrows in the blue solid curves indicate the direction of propagation and the dashed circles, whose centres are represented by circular dots, correspond to circles fitted to $\langle\vec{r}\rangle$.

into the magnetic barrier and, for $B_0 = 15$ T, it does not even reach the barrier region. In fact, for a stronger magnetic field, the effect of this field on the upper part of the wavepacket is more pronounced, leading to a stronger distortion of the packet. In addition, figure 5(b) shows that, decreasing the effective mass, the wavepacket becomes more susceptible to the magnetic field and the centre of mass penetrates less into the magnetic field region (shaded region in the figure). Notice that, for $B_0 = 5$ T, the centre of mass of the wavepacket with effective mass $m = 0.01m_0$ does not penetrate the barrier,

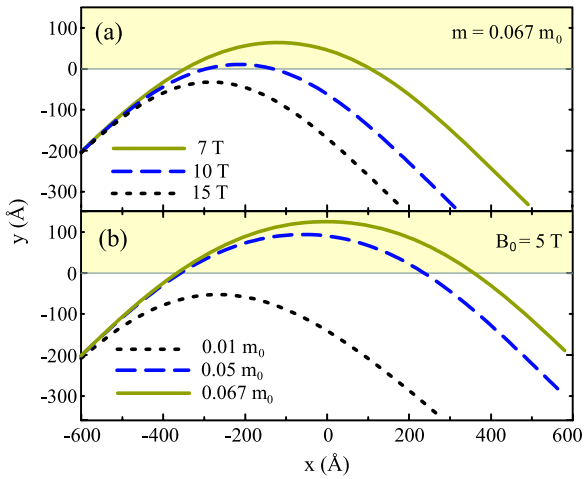

Figure 5. Trajectory of the electron wavepacket with parameters $d = 100$ Å and $E = 100$ meV for (a) an effective mass $m = 0.067m_0$ and different values of magnetic field barrier height B_0, and (b) a barrier height $B_0 = 5$ T for several values of the effective mass. The shaded area corresponds to the region of non-zero magnetic field.

making it very different from the classical trajectory. The contour plots of the wavefunctions at different time steps for $B_0 = 5$ T, shown in figure 6, illustrates the trajectory of the wavepacket for the case $m = 0.01m_0$ shown in figure 5(b), which helps us to understand the large discrepancy between $\langle\vec{r}\rangle$ and the classical trajectories. Indeed, only the upper part of the packet penetrates the barrier, scattering back and interfering with the large portion of the wavepacket that remains out of the barrier. Therefore, when we average over the wavepacket in order to obtain the centre-of-mass position, it appears outside the barrier region.

3. Wavepacket dynamics in graphene

In graphene, the low-energy electron states in the vicinity of the K point of the first Brillouin zone are described by massless Dirac fermions with the Hamiltonian

$$H_{\mathrm{D}} = v_{\mathrm{F}}\vec{\sigma}\cdot\left(\vec{p} - e\vec{A}\right) + V(x,y)\mathbf{I} + M(x,y)\sigma_z, \qquad (13)$$

where $\vec{\sigma}$ is the usual Pauli vector, $\mathbf{I}$ is the 2×2 identity matrix and the wavefunctions are written as pseudo-spinors $\Psi = (\Psi_A, \Psi_B)^T$, where Ψ_A (Ψ_B) is the probability amplitude of finding the electron in the sub-lattice A (B) of graphene [8]. In the presence of a non-zero mass term $M(x, y)$, the energy spectrum exhibits a gap, thus a space-dependent mass is often considered to create a landscape of energy gaps and simulate electron confinement [35]. The magnetic field $\vec{B} = B(x, y)\hat{z}$ enters the Hamiltonian through the vector potential $\vec{A} = (A_x, A_y, 0)$, where $\vec{B} = \vec{\nabla}\times\vec{A}$. For the K′ point, one must replace $\vec{\sigma}$ by its complex conjugate $\vec{\sigma}^*$ in equation (13). Since the results for the K′ point can be straightforwardly inferred

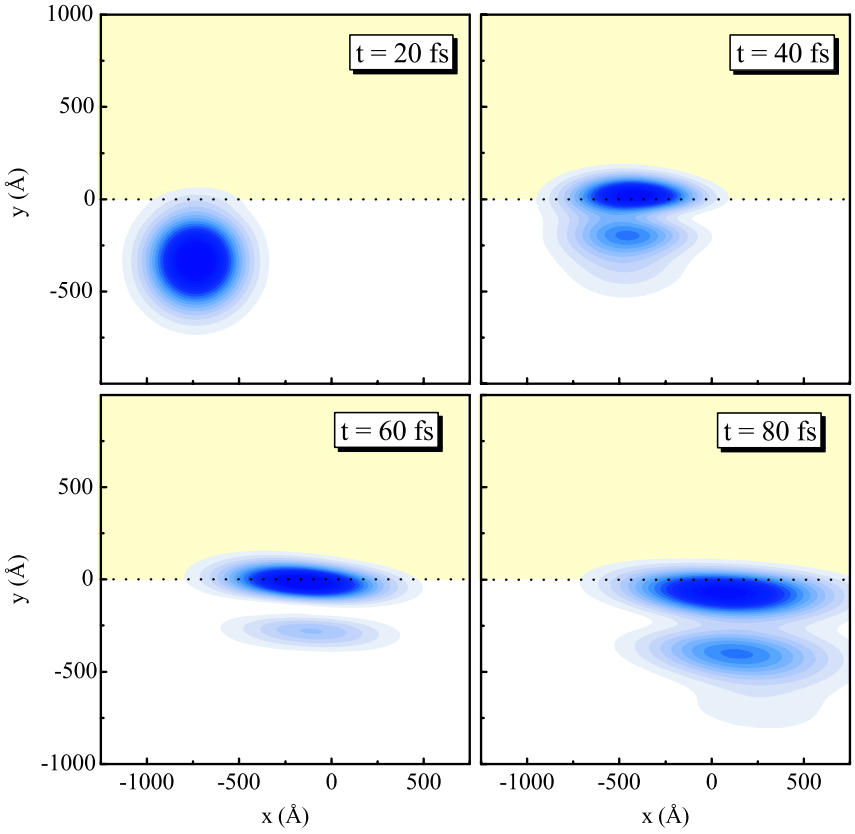

Figure 6. Contour plots of $|\Psi|^2$ at four different time steps for a Schrödinger particle with effective mass $m = 0.01m_0$ scattered by a magnetic field step barrier $B_0 = 5$ T, represented by the shaded area (see figure 5(b)). Darker (lighter) colours represent higher (lower) values of the probability density.

from those for the K point and, as we are dealing only with ideal infinite graphene sheets, i.e. in the absence of intervalley scattering due to impurities, defects or edge effects, we will hereafter consider only the case of electrons in the vicinity of the K point.

Following the split-operator scheme, the time-evolution operator equation (1) for the Dirac Hamiltonian H_{D} can be rewritten as

$$\exp\left[-\frac{\mathrm{i}}{\hbar}H_{\mathrm{D}}\Delta t\right] = \mathrm{e}^{-\mathrm{i}\vec{\varrho}\cdot\vec{\sigma}}\mathrm{e}^{-\mathrm{i}\vec{\kappa}\cdot\vec{\sigma}}\mathrm{e}^{-\mathrm{i}\vec{\varrho}\cdot\vec{\sigma}} + \mathrm{O}(\Delta t^3), \tag{14}$$

where $\vec{\varrho} = \frac{\Delta t}{2\hbar}[(v_{\mathrm{F}}eA_x, v_{\mathrm{F}}eA_y, M) + V\mathbf{I}]$, $\vec{\kappa} = \Delta t v_{\mathrm{F}}\vec{k}$ and $\vec{k}$ is the wavevector. The $\mathrm{O}(\Delta t^3)$ error is a consequence of the non-commutativity between $\vec{\varrho}$ and $\vec{\kappa}$.

The exponentials can be expressed in terms of the matrices $\mathcal{M}_r$ and $\mathcal{M}_k$, written in the space of position and momenta, respectively, as

$$\mathcal{M}_r = \left[\cos(\varrho)\mathbf{I} - \mathrm{i}\frac{\sin(\varrho)}{\varrho}\begin{pmatrix}\mathsf{M} & \mathsf{A}_x - \mathrm{i}\mathsf{A}_y\\ \mathsf{A}_x + \mathrm{i}\mathsf{A}_y & -\mathsf{M}\end{pmatrix}\right]\mathrm{e}^{-\frac{\mathrm{i}\Delta t}{2\hbar}V}, \tag{15a}$$

$$\mathcal{M}_k = \cos(\kappa)\mathbf{I} - \mathrm{i}\frac{\sin(\kappa)}{\kappa}\begin{pmatrix}0 & \kappa_x - \mathrm{i}\kappa_y\\ \kappa_x + \mathrm{i}\kappa_y & 0\end{pmatrix}, \tag{15b}$$

where $\kappa = |\vec{\kappa}| = \Delta t v_{\mathrm{F}}|\vec{k}|$, $\varrho = |\vec{\varrho}| = |(\mathsf{A}_x, \mathsf{A}_y, \mathsf{M})|$ and we define the dimensionless quantities $\vec{\mathsf{A}} = \Delta t v_{\mathrm{F}}e\vec{A}/2\hbar$ and $\mathsf{M} = \Delta t M/2\hbar$. These expressions generalize those presented in [32] and [26], taking into account both the mass term and the external magnetic field.

Now we can obtain the wavefunction at a posterior time starting from an initial wavefunction as

$$|\Psi\rangle_{t+\Delta t} \cong \mathcal{M}_r \cdot \mathcal{M}_k \cdot \mathcal{M}_r \cdot |\Psi\rangle_t, \tag{16}$$

where terms of order higher than Δt^2 are neglected, and where before (afterwards) the multiplication of the matrix $\mathcal{M}_k$, we must perform a direct (inverse) Fourier transform on the function, in order to map it to reciprocal (real) space. Note that, in the absence of external fields, if the Hamiltonian has neither external potentials nor mass terms, that is, $\vec{B} \equiv 0$, $V(x, y) \equiv 0$ and $M(x, y) \equiv 0$, the separation between the real and reciprocal space-dependent terms in equation (14) is no longer necessary, and the multiplication of the initial wavefunction by the matrix $\mathcal{M}_k$, defined by equation (15*b*), gives the exact solution of the time evolution of the wavepacket for any value of Δt. However, in the case where $V(x, y)$ or $M(x, y)$ is non-zero, or in the presence of magnetic fields, the $\mathrm{O}(\Delta t^3)$ error induced by the non-commutativity of the terms of the Hamiltonian restricts the method to the use of small values of Δt.

As mentioned above, the wavefunction in graphene must be written as a pseudo-spinor. Thus our initial wavepacket in this case is slightly different from the one in equation (8) and is given by

$$\Psi(x, y) = \begin{pmatrix}\Psi_A\\ \Psi_B\end{pmatrix} = \frac{1}{d\sqrt{2\pi}}\exp\left[-\frac{(x - x_0)^2}{2d^2} - \frac{(y - y_0)^2}{2d^2} + \mathrm{i}\vec{k}^{(0)}\cdot\vec{r}\right]\begin{pmatrix}c_1\\ c_2\end{pmatrix}, \tag{17}$$

where d is the width of the wavepacket, the wavevector is related to the energy as $|\vec{k}^{(0)}| = k^{(0)} = E/\hbar v_{\mathrm{F}}$ and the pseudo-spinor of the initial wavepacket is chosen as [5] $c_1 = 1$, $c_2 = \mathrm{i}\mathrm{e}^{-\mathrm{i}\varphi}$. By calculating the expectation values $\langle\sigma_x\rangle$ and $\langle\sigma_y\rangle$ with the wavefunction equation (17), one straightforwardly identifies φ as the pseudo-spin polarization angle of the initial wavepacket, measured from the vertical axis, i.e. $\varphi = 0$ represents a pseudo-spin polarization in the y direction.

The trajectory of the centre of mass $\langle\vec{r}\rangle$ of a Dirac wavepacket is calculated by computing

$$\langle\vec{r}\rangle = \langle\Psi|\vec{r}|\Psi\rangle = \int(\Psi_A^*\Psi_A + \Psi_B^*\Psi_B)\vec{r}\,\mathrm{d}^2r \tag{18}$$

for each time step. The propagation velocity can be calculated either by taking the time derivative of $\langle x\rangle$ and $\langle y\rangle$ as in equation (10), or by computing the expectation value of the pseudo-spinor for each time step, as follows from the Heisenberg picture:

$$\vec{v}(t) = \frac{\mathrm{d}\langle\vec{r}\rangle}{\mathrm{d}t} = \frac{1}{\mathrm{i}\hbar}[\vec{r}, H] = v_{\mathrm{F}}\vec{\sigma}(t). \tag{19}$$

As the propagation velocity vector and the pseudo-spin vector point to the same direction, the pseudo-spin polarization angle φ of the initial wavepacket can also be identified as the angle of propagation of this wavepacket.

The dynamics of wavepackets for Dirac particles exhibits non-trivial features that will be discussed in the following subsections.

3.1. Scattering by a mass barrier and zitterbewegung

Wavepackets describing Dirac particles are composed of a distribution of energy (and consequently momentum) states, which can have positive or negative values. Besides, from the Heisenberg picture, we observe that the propagation velocity depends on the expectation value of the Pauli matrices σ_x and σ_y (see equation (19)). This leads to two consequences: (i) the propagation direction depends on the (pseudo) spin polarization of the initial wavepacket, and (ii) as the Pauli matrices do not commute with the Hamiltonian equation (13), they are not constants of motion and, consequently, the velocity changes in time, even in the absence of external forces, giving rise to the so-called zitterbewegung, or trembling motion [12].

As we mentioned earlier, from the velocity equation (19), we observe that the Dirac wavepacket propagates in the direction of its initial (pseudo) spin polarization. For example, a wavepacket with pseudo-spin polarization angle $\varphi = 0$, i.e. $c_1 = 1$ and $c_2 = \mathrm{i}$ (and $\vec{k}^{(0)} = k^{(0)}\hat{y}$), propagates in the y direction, whereas its x component remains constant. Even so, the velocity in the propagation direction exhibits an oscillation which is damped as the time evolves, since $[\sigma_y, H_{\mathrm{D}}] \neq 0$ and, consequently, v_y is not a constant of motion. Such oscillations are shown in figure 7, where the inset shows the coincidence of the results obtained from $\frac{\mathrm{d}\langle y\rangle}{\mathrm{d}t}$ (solid line) and from $\langle\sigma_y\rangle$ (symbols). The different curves in figure 7 are the results for different mass-related potential backgrounds $M(x, y) \equiv M_0$, showing that the presence of such a mass term has a strong influence on the zitterbewegung: as M_0 increases,

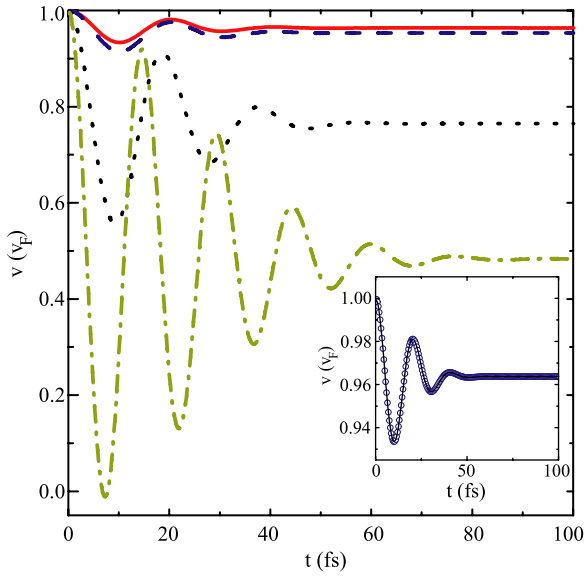

Figure 7. Velocity of a free wavepacket in a graphene layer as a function of time, obtained from $\frac{d\langle y\rangle}{dt}$, in a system with different values of mass-related potential $M_0 = 0$ (solid), 10 (dashed), 50 (dotted) and 100 meV (dashed–dotted). The initial wavepacket has average energy $E = 100$ meV, pseudo-spin polarization $\varphi = 0$ and width $d = 200$ Å. Inset: velocity obtained from $\frac{d\langle y\rangle}{dt}$ (solid line) and $\langle\sigma_y\rangle$ (symbols) for the $M_0 = 0$ case.

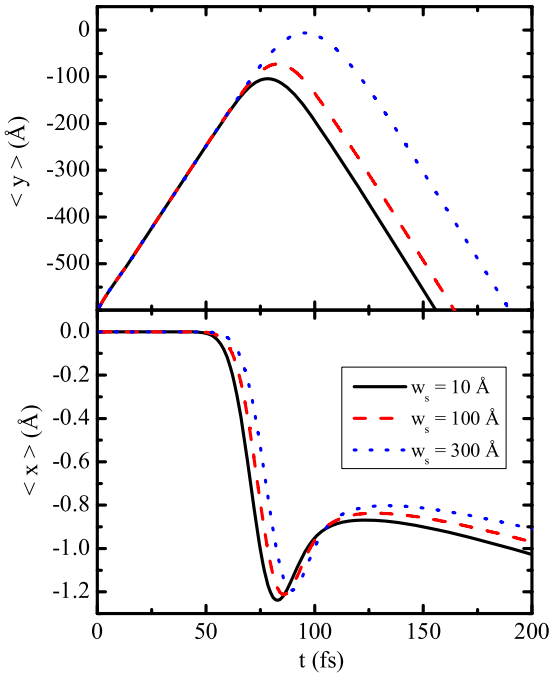

Figure 8. Expectation values of x and y as a function of time for a wavepacket with energy $E = 100$ meV and width $d = 100$ Å, scattered by a mass step barrier with a gap $M_0 = 300$ meV. We consider a smooth step barrier, with a linear interface with thickness w_s.

the amplitude of oscillation increases and its period is reduced. This is expected, since the inclusion of a mass term leads to a non-zero σ_z term in H_D and, as $[\sigma_y, \sigma_z] \neq 0$, this additional term does not commute with the velocity v_y; consequently the final velocity will exhibit stronger oscillations. This shows that the presence of a mass-related potential will be helpful for the experimental visualization of the zitterbewegung in graphene. Such a term can be realized with state-of-the-art techniques. Recent experiments [28] have reported the deposition of a graphene layer over a substrate that produces a site-dependent potential V_A (V_B) on the atoms of the sublattice A (B). Within the Dirac approximation, this potential is translated into a mass term in H_D. Previous papers about the substrate-induced potential in graphene focused on the opening of an energy gap by such a potential. Here, we show that this term not only opens a gap, but also intensifies significantly the zitterbewegung effect.

As we mentioned, the velocity oscillates in time (due to the zitterbewegung) but converges to a constant. For a massless fermion, this constant can be obtained analytically from equations (31) of Maksimova *et al* [5]:

$$\bar{v}_x = \frac{1 - e^{-a^2}}{2a^2}\cos\varphi, \qquad \bar{v}_y = \left(1 - \frac{1}{2a^2} + \frac{e^{-a^2}}{2a^2}\right)\sin\varphi, \tag{20}$$

where a is the dimensionless parameter $a = k^{(0)}d$ (for more details, see [5]). Our numerical results reproduce the analytical results of Maksimova *et al* for the case with no magnetic, potential or mass terms included. This confirms that, in this case, our numerical time-evolution method is exact, i.e. there is no error induced by non-commutative terms. As we have a wavepacket, we can choose some value of E far from the Fermi level $E = 0$, but there will always be a distribution in energy space with width $d_k \propto d^{-1}$ and, hence, there will always be a non-zero projection of the wavepacket on the states with negative E (or negative k). Because of this, the zitterbewegung effect occurs and has an influence on the final velocity of the packet, which is always found to be $v_y < v_F$, as one can verify from equation (20). Indeed, for higher energies or broader wavepackets, the projection over these states is reduced, the zitterbewegung is weaker and the final velocities in equation (20) approach $v_y \approx v_F$.

The enhanced zitterbewegung due to the mass term brings us to the discussion of the possibility of using mass barriers to simulate the borders of a graphene flake. In [35], for instance, a circular mass barrier was considered in order to simulate a graphene quantum dot, where it was demonstrated that good qualitative agreement with some experimental data can be obtained. As a matter of fact, the electron should not be able to go through the graphene edge, and this edge acts as an infinite gap. In this way, we could naively think that simply considering an infinite mass region, i.e. generating an infinite gap, we would be able to describe precisely the scattering of a wavepacket at the border of a graphene sheet. This, however, is wrong, since the mass term not only opens the gap but also has an influence on the zitterbewegung, as we just demonstrated.

In order to illustrate this, let us consider as an example the scattering of an $E = 100$ meV and $d = 100$ Å wavepacket by a mass barrier in the y direction, which we take as smooth, so that the mass-related potential is zero for $y < 0$ but increases linearly from $M = 0$ to 300 meV in the interval $0 < y < w_s$.

This mass barrier height was chosen based on the gap found experimentally for a graphene sheet over an SiC substrate [28]. Figure 8 shows the average coordinate values $\langle y\rangle$ and $\langle x\rangle$ of this wavepacket as a function of time for several values of the interface thickness w_s. The y position of the wavepacket starts to decrease after the packet is reflected by the mass step barrier, due to the gap opening by the mass term. For larger interfaces, the wavepacket clearly penetrates more into the barrier region ($y > 0$) and it takes longer to be completely reflected. Either classical particles or Schrödinger particles are not expected to exhibit any motion in the x direction in this situation. Besides, in the absence of a mass term, the studied wavepacket should exhibit no oscillation due to the zitterbewegung in the x direction, since we have chosen both the pseudo-spin polarization and the momentum in the y direction. The former guarantees that the propagation velocity is initially in the y direction, according to equation (19), whereas the latter leads to $k_x^{(0)} = 0$ and, as k_x is a constant of motion, the wavevector stays in the y direction during the whole propagation. Indeed, in the beginning of the motion, where $M = 0$, $\langle x\rangle$ stays close to zero. However, when the wavepacket reaches the region where $M \neq 0$, i.e. when the packet starts to be reflected, the x position of the packet starts to oscillate due to the zitterbewegung, induced by the additional $M\sigma_z$ term in the Hamiltonian at this region. For larger interface thickness, this oscillation in $\langle x\rangle$ becomes less significant, but it stays clearly visible even for $w_s = 300$ Å. Notice that this oscillation is not symmetric around $x = 0$. This apparent symmetry breaking is a common feature of zitterbewegung, which is also observed, for example, in figures 2 and 4 of [5]. However, if one considers either electrons in the K′ Dirac cone or a negative mass term $M(x, y) \to -M(x, y)$ (which leads to the same energy gap), $\langle x\rangle$ would perform oscillations in the opposite way. Interestingly, the reflected wavepacket keeps drifting to the x direction even after the reflection, which suggests that the mass-related zitterbewegung should be observable experimentally by analysing the initial and final positions of the propagating wavepacket.

3.2. Scattering by a potential barrier—Klein tunnelling

Let us now analyse the wavepacket dynamics in a potential step barrier of height V_0, defined as $V = V_0\Theta(y)$. Classically, it is well known that, if the incident particle has an energy which is lower than the barrier height, it is reflected, whereas for an energy larger than V_0 it is transmitted over the barrier. On the other hand, in the 2DEG discussed in section 3.1, where particles are described by the Schrödinger equation, the particle still has a finite probability of being reflected. In the case of graphene, where the quasi-particles obey the Dirac equation, something even more curious occurs: for perfectly normal incidence on the potential barrier step (that is, $k_x = 0$ and $k_y > 0$), the particle is always fully transmitted, no matter if its energy is higher or lower than the barrier height. This occurs because, even if the electron energy is lower than the potential height, it can still tunnel through the barrier region as a hole state, as illustrated in figure 9. This is the so-called Klein tunnelling [32, 36]. In the case of the wavepacket considered

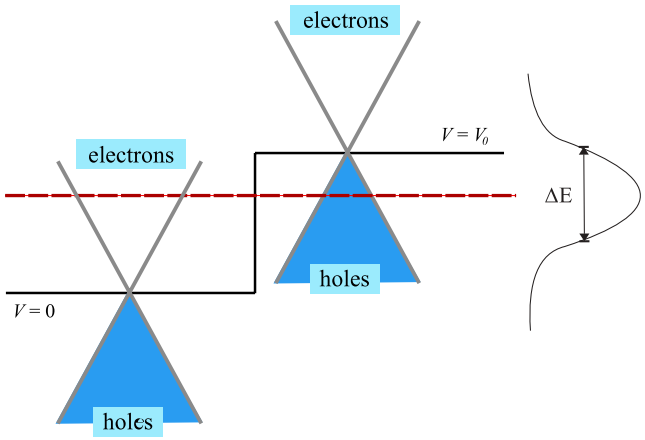

Figure 9. Sketch that illustrates the Klein tunnelling: an electron in a Dirac cone with energy E (red dashed line) lower than the potential step height V_0 (black line) propagates in the barrier region as a hole state, if its incidence is normal to the barrier. The Gaussian curve on the right side of the figure represents the energy distribution of the wavepacket, with width $\Delta E = \hbar v_F \Delta k$.

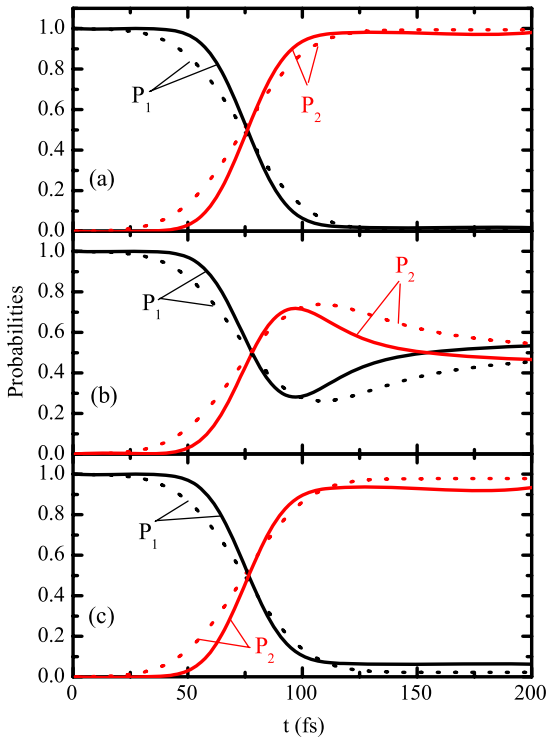

Figure 10. Probability of finding the Dirac particle outside (P_1, black) and inside (P_2, red) the barrier as a function of time, for different potential heights $V_0 = 0$ (a), 110 meV (b) and 250 meV (c). The wavepacket propagates in the y direction ($\varphi = 0$), with energy $E = 100$ meV, and two values of the wavepacket width are considered: $d = 150$ Å (solid) and 250 Å (dotted).

in this work, there is a momentum distribution of width $\hbar\Delta k_x$, inversely proportional to Δx. Thus, we cannot expect perfect transmission in our case, as we are not dealing exactly with normal incidence. Even so, the results in figure 10 exhibit a high transmission probability, if the wavepacket energy is far below the barrier height V_0. Figure 10 shows the probabilities

of finding the particle outside (P_1) and inside (P_2) the barrier region, where $P_1 + P_2 = 1$, as a function of time for different potential heights $V_0 = 0$ (a), 110 meV (b) and 250 meV (c). The parameters defining the wavepacket are $E = 100$ meV and $d = 150$ Å (solid) and 250 Å (dotted). In figure 10(a) we plot the case where $V_0 = 0$ just as a guide, to show at which time the packet should be passing through each region in the absence of the potential barrier. For V_0 close to E, the transmission probability P_2 decreases, converging to ≈0.45 (≈0.55) for a wavepacket width $d = 150$ Å (250 Å). This strong reflection, in contrast to the otherwise perfect transmission for Dirac particles expected due to the Klein tunnelling, is explained by the fact that we have a Gaussian distribution of momentum in the x direction so that, although the $k_x = 0$ state should pass without reflection, all the remaining states that compose the Gaussian distribution should undergo some reflection, since they have $k_x \neq 0$. The comparison between the results with $d = 150$ Å (solid) and 250 Å (dotted) helps to support this idea: narrower wavepackets exhibit lower P_2 as $t \to \infty$, since it has a larger distribution of momentum in the k_x direction, i.e. a larger part of the packet must be reflected due to its non-normal incidence. Considering a higher potential barrier $V_0 = 250$ meV, the Klein tunnelling is much more evident and the differences between the probabilities for the $d = 100$ and 200 Å wavepackets are minimized, as one can observe in figure 10(c), where the curves are very similar to the $V_0 = 0$ case shown in figure 10(a). It is clearly seen that the wavepacket is practically fully transmitted through the barrier ($P_2 \to 1$) for the $d = 250$ Å (dotted) case, whereas for $d = 150$ Å (solid) it still undergoes a very small reflection due to the $k_x \neq 0$ states in the wavepacket, as discussed above.

In fact, when the electron energy is close to the barrier height, the window of incident angles for which the transmission probability is maximum is much narrower. This effect is well known and explains the large lifetime of quasi-bound states with energy close to the barrier height in graphene circular quantum dots [21, 37]. Figure 11 shows the transmission probability P_2 as a function of time and barrier potential height V_0 for the same wavepackets as in figure 10, considering $d = 150$ Å (a) and 250 Å (b). As we are considering $k_x^{(0)} = 0$, i.e. normal incidence, the transmission probability reaches practically 1 for almost any potential height, but exhibits a minimum for $V_0 = E = 100$ meV. This minimum comes from the reflection of the $k_x \neq 0$ part of the momentum distribution of the wavepacket, which is larger for $V_0 = E$ because in this case full transmission due to Klein tunnelling occurs only for perfectly normal incidence angle. Indeed, as the $d = 250$ Å wavepacket has narrower k_x distribution around $k_x^{(0)} = 0$, its minimum in figure 11(b) is narrower as compared to the one for $d = 150$ Å in figure 11(a). This result also explains why a much stronger reflection was observed in figure 10(b), where the barrier height is closer to the wavepacket energy.

The contour plots of the squared modulus of the wavefunction scattered by the $V_0 = 110$ meV potential in figure 12 illustrates what we explained: for $t = 180$ fs, the reflected wavefunction exhibits a line of zeros in $x = 0$, which supports the idea that every part of the wavepacket

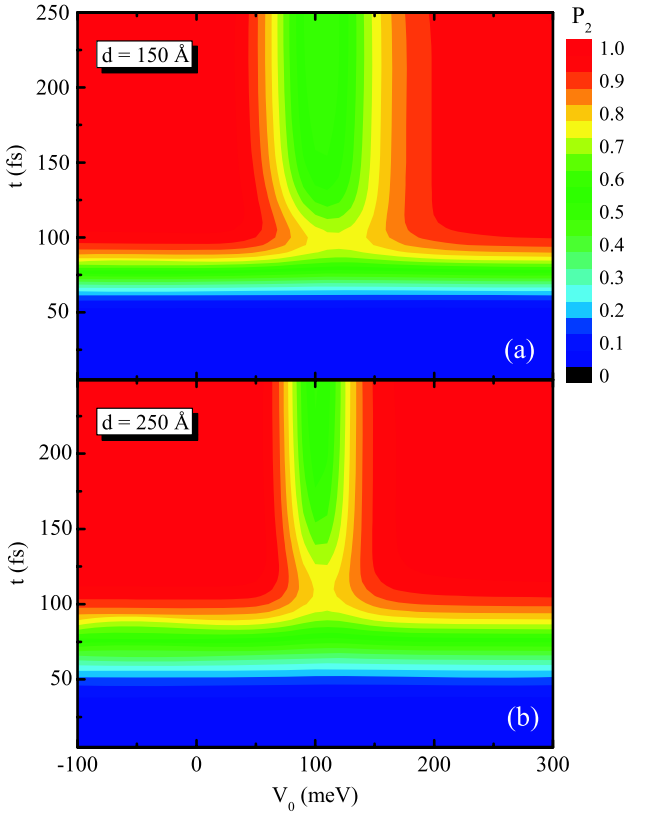

Figure 11. Probability P_2 of transmitted wave, as a function of time and barrier height potential, for a wavepacket with energy $E = 100$ meV, pseudo-spin polarization angle $\varphi = 0$, and widths $d = 150$ Å (a) and 250 Å (b).

that has normal incidence at the step barrier is transmitted, so that only the $k_x \neq 0$ parts are reflected, propagating towards the diagonal directions of the plane. In other words, the $k_x \approx 0$ states, which would fill the space in between the two parts of the reflected wavepacket, are fully transmitted through the barrier due to the Klein tunnelling. For a wavepacket energy E far below the barrier height V_0, there is a larger window of values of k_x around $k_x = 0$ with high transmission probabilities, which leads to a larger separation between the two parts of the reflected wavepacket, but also to a smaller reflection probability, as already demonstrated by the results in figures 10(c) and 11.

Notice that the way we are investigating the Klein tunnelling is different from the one usually studied in the literature [8, 37], since we are not dealing with a particle with a singly defined momentum, but with a wavepacket with a momentum distribution instead. In fact, we already demonstrated that these two points of view lead to essentially different results: Klein tunnelling is not always fully observed if one considers a wavepacket. However, there is something else to be observed: for a wavepacket propagating inside the barrier with E close to V_0, the admixture of electron and hole states (see figure 9) is much stronger than outside the barrier. This explains why the transmitted wavepacket in figure 12 becomes so distorted as time goes on, which does not happen for such a wavepacket in the absence of the

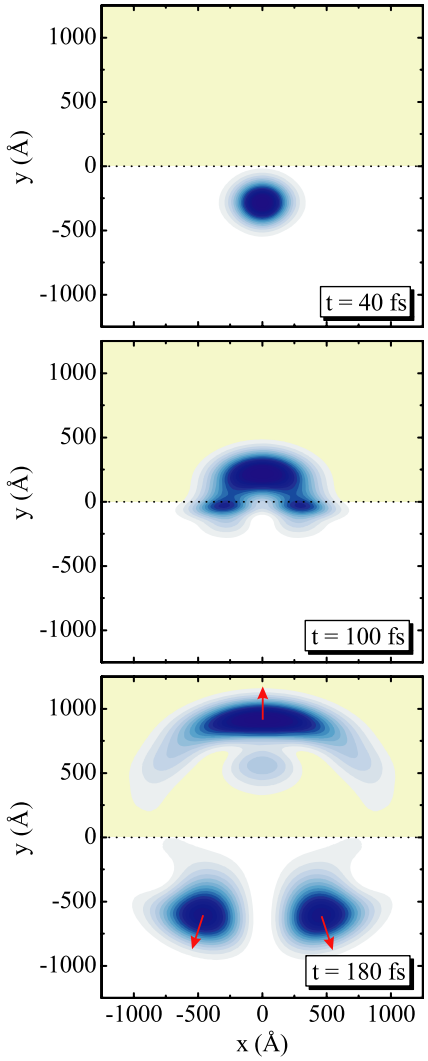

Figure 12. Contour plots of $|\Psi|^2$ scattered by a $V_0 = 110$ meV step barrier potential for three different instants in time. The shaded area corresponds to the non-zero potential region. Darker (lighter) colours represent higher (lower) values of the probability density. The initial wavepacket has energy $E = 100$ meV, width $d = 150$ Å and propagates in the y direction ($\varphi = 0$).

potential. Actually, for a wavepacket energy close to $E = 0$, where such an admixture also occurs, this distortion is also observed [5]. As demonstrated in figure 7, the zitterbewegung is a transient effect [16], so that the wavefunction exhibits damped oscillations. However, as the packet penetrates a region with a different potential landscape, the zitterbewegung is re-activated and can also be observed in the shape of the transmitted wavepacket, which is not preserved in time.

Figure 13 shows contour plots of the cross section at $x = 0$ of the squared modulus (top) and the real part (bottom) of the wavefunction as a function of time, for a wavepacket with $E = 100$ meV and $d = 200$ Å and with normal incidence at a step barrier potential $V_0 =$ (a) 0, (b) 110 and (c) 250 meV. The inset in the $V_0 = 110$ meV case shows the tunnelled wavefunction profile at $t = 170$ fs, where we observe the distortion in the y direction due to the interference between electron and hole states. This distortion in the shape of the wavepacket is analogous to the one observed in figure 12 for $t = 180$ fs, which is explained as being due to a re-activated zitterbewegung after penetration into the barrier region. In fact, this is the only case where the tunnelled wavefunction does not preserve its initial shape, with a single peak; for the other two values of V_0, where there is less admixture between positive and negative energy states inside the barrier, the tunnelled wavefunction stays approximately with the same shape during the whole propagation. For $V_0 = 250$ meV, where the wavepacket energy is much smaller than the barrier height, the tunnelled packet is practically fully distributed among hole states, which have negative momenta. This affects the phase velocity, namely the variation of the peaks of $\mathrm{Re}[\Psi(0, y)]$ as a function of time: although the wavepacket itself keeps propagating towards the positive y direction, these peaks start to propagate in the opposite direction when the packet penetrates the barrier, due to the negative momenta (hole) states in this region. This result just confirms that the wavepacket studied in this work really undergoes all the effects inherent to Klein tunnelling for $V_0 = 250$ meV: its transmission probability approaches 1 (see figure 11(b)) and this is really due to the 'transformation' of the initial electron state into a hole state inside the barrier (see figure 13).

Finally, another feature of figure 13 which is worth discussing regards the fact that the wavepacket does not change its velocity significantly when it tunnels through the barrier. Actually, this velocity slightly changes just because of the large distribution of momenta in the x direction (perpendicular to the motion) of this wavepacket, so that zitterbewegung effects make the final velocity turns out smaller than v_F, obeying equation (20). If we consider an infinitely wide wavepacket in the x direction, its velocity when it penetrates the barrier does not change at all. Velocity modulations due to tunnelling effects and even 'superluminal' velocities of tunnelling particles in graphene, also known as the Hartman effect [38], have been predicted in previous papers [39, 40]. The Hartman effect, namely the superluminal velocity acquired by some tunnelling particles, was first suggested for photons tunnelling through the gap between two prisms, but has also been expected to be observed with electrons tunnelling through potential barriers in graphene, where the tunnelling probability is very high due to the Klein paradox. However, our results demonstrate that, at least in the framework of wavepackets, Klein tunnelling does not lead to the Hartman effect, which is in accordance with [41].

3.3. Scattering by magnetic barriers

In section 2.2 we analysed the trajectories of Schrödinger particles travelling through a magnetic barrier, where we observed that, decreasing the electron effective mass m, one can reduce the radius of the circular trajectories and even push the packet out of the barrier, so that it is reflected before its centroid reaches the magnetic field region. In this section, we analyse the trajectories of massless Dirac particles in a similar magnetic field barrier.

Figure 14(a) shows the trajectory of the centre of mass $\langle \vec{r} \rangle$ for different widths d of the wavepacket, considering

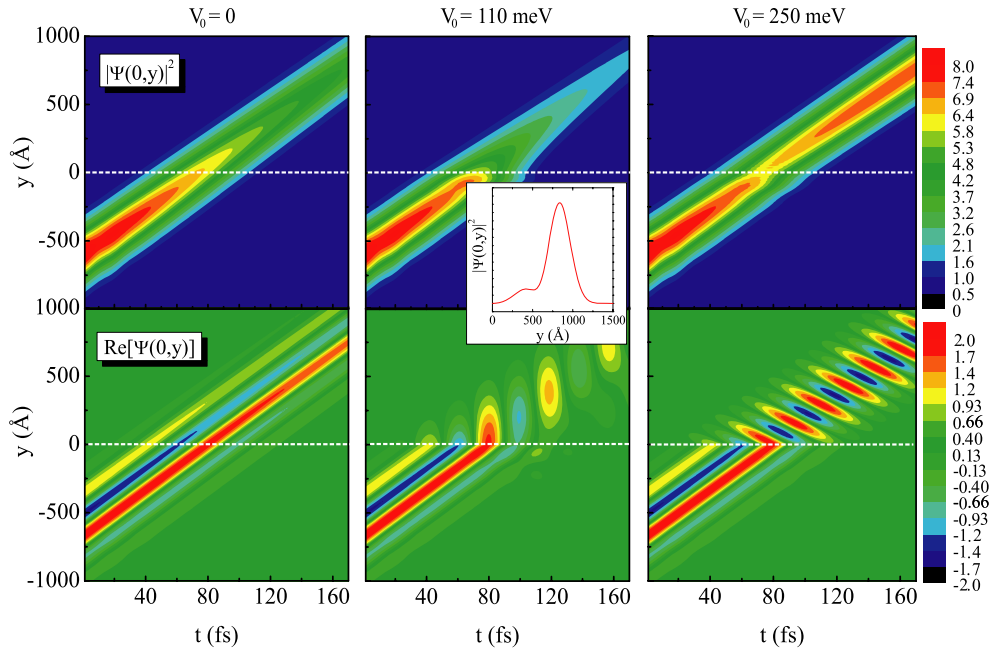

Figure 13. Contour plots of the cross section of the squared modulus (top) and the real part (bottom) of the wavefunction at $x = 0$ as a function of time, for a wavepacket propagating in the y direction ($\varphi = 0$). We consider a step barrier potential $V = V_0\Theta(y)$ for three values of V_0. The dotted horizontal line delimits the potential barrier interface. The inset shows the squared modulus of the cross section of the wavefunction $|\Psi(0, y)|^2$ at $t = 170$ fs for $V_0 = 110$ meV.

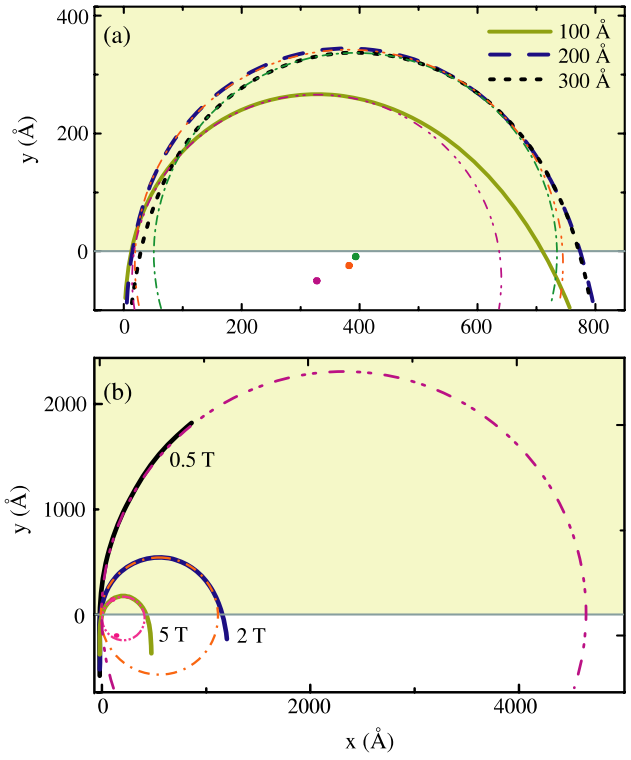

Figure 14. Trajectory of the centre of mass of the wavefunction in graphene, propagating in the vertical direction ($\varphi = 0$) (a) for different sizes of the wavepacket d, considering a magnetic field barrier height $B_0 = 3$ T and (b) for various intensities of the external magnetic field B_0, considering an initial wavepacket width $d = 200$ Å. The shaded areas correspond to the non-zero magnetic field region and the wavepacket energy in all the cases is assumed as $E = 100$ meV.

Table 1. Analysis of the circles describing the trajectory of a wavepacket in graphene in the presence of a magnetic field barrier of height $B_0 = 5$ T. We compare the radius obtained by solving the Dirac equation (R_N) to the radius obtained from the classical expression (R_c). The centre of the numerically obtained circles is O(x, y), which should be compared to O(R_c, 0) in the classical approximation.

d (Å)	O(x, y)	R_N (Å)	R_c (Å) ($\frac{v}{v_F}$)
100	(200, −62)	188	284 (0.859)
150	(220, −37)	204	261 (0.935)
200	(228, −28)	203	254 (0.964)

perpendicular incidence to a magnetic field step of height $B_0 = 3$ T. As the width of the packet increases, the packet penetrates deeper in the magnetic field region. Also, figure 14(b) shows the trajectory of the centre of mass in the case $d = 200$ Å for different values of the height of the magnetic field step B_0. As the magnetic field increases, the radius of curvature is reduced, as expected from the Lorentz force, and there is less penetration into the magnetic field region. We fitted circles to the numerically obtained trajectories in the barrier region, which are shown as dashed–dotted lines, in order to compare with the classical result, where the particle should exhibit a circular trajectory with radius $R_c = E/evB$ inside the barrier region. Similarly to the Schrödinger case, the circles are fitted to the numerically obtained trajectories and have not only different radii R_N as compared to their respective R_c, but also their centres O = (x_c, y_c) (circular dots) are displaced from the classical point $O_c = (R_c, 0)$.

A collection of values of O and R_N, for $B = 5$ T and different values of wavepacket width d, is shown in table 1,

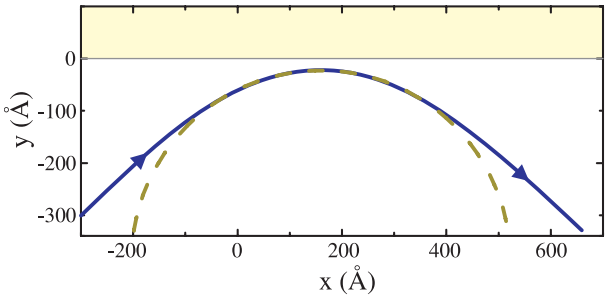

Figure 15. Trajectory of the centre of mass of the wavepacket with $d = 200$ Å and $E = 100$ meV in graphene, propagating with an angle $\varphi = \pi/4$ and being reflected by a magnetic field barrier $B_0 = 5$ T, represented by the shaded area. The arrows indicate the direction of propagation.

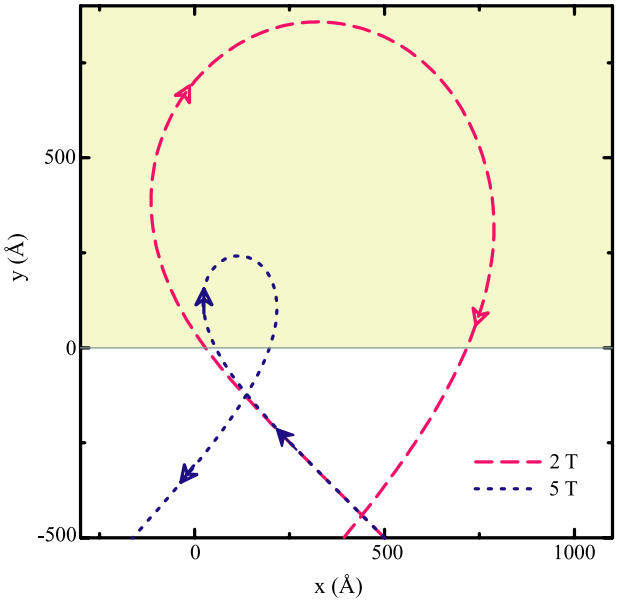

Figure 16. The trajectory of the centre of mass of the wavepacket with $E = 100$ meV and $d = 200$ Å, with propagation angle $\varphi = -\frac{\pi}{4}$ in a magnetic field step barrier in graphene, for two different magnetic barrier heights.

where we observe that as d increases, i.e. as the wavepacket approximates the limit where it has a single momentum state, the differences between the quantum and classical results are reduced. Notice that we are using the numerically obtained wavepacket velocities v to calculate the classical orbits. These velocities differ from the Fermi velocity v_F and depend on the wavepacket width d according to equation (20). Consequently, the radius of the trajectory must depend on the wavepacket width too. The radius obtained by substituting the Fermi velocity in the classical expression is 244 Å.

For slanted incidence, the results are quite analogous to those of the Schrödinger case studied in section 2.2. Nevertheless, we show in figure 15, as an example, the trajectory of the wavepacket for the case $\varphi = \pi/4$, in graphene, considering a magnetic field barrier height $B_0 = 5$ T, where we observe that the centre of mass of the wavepacket (solid) does not even penetrate the magnetic barrier region. The centre of the circle fitted to the scattering part of this trajectory (dashed) is clearly below the classical one, which has its centre at $y = 0$. Equivalently to the Schrödinger case, this is a manifestation of the non-zero width of the wavepacket and its resulting interference, so that the contour plots of the wavefunctions reflected by the magnetic barrier exhibit the same features as shown in figure 6 which, thus, will not be repeated here. Notice that in the case of graphene, in contrast to the Schrödinger case, choosing a wavevector $\vec{k}^0$ pointing in a tilted direction with an angle φ is not enough for slanted propagation; one must also substitute the angle φ in the pseudo-spinor in equation (17) in order to observe such a propagation.

Notice that, as the magnetic barrier interface is in the x direction, it is easy to verify that the incidence angle (measured from the normal direction) coincides with the propagation angle of the wavepacket φ. When the particle reaches the magnetic barrier with incidence angle $\varphi = \frac{\pi}{4}$, the magnetic field makes it travel onto a circle in the clockwise direction, as observed in figure 15 and verified by the right-hand rule. This is also true when the incidence angle is $\varphi = -\frac{\pi}{4}$, hence, in this situation, the trajectory of the particle inside the magnetic barrier must make a loop. Indeed, such a loop is observed in $\langle\vec{r}\rangle$ for this situation in figure 16, but the loops are not perfect circles in contrast to the results from a classical calculation. The contour plots of the wavefunction in figure 17 help to explain why: in these cases, only part of the wavepacket performs a circular trajectory, while the other part is still below the magnetic barrier and hence does not interact with the field, leading to a spurious distortion in the circular trajectory of $\langle\vec{r}\rangle$.

As we know that the trajectories of wavepackets in a magnetic field barrier in graphene obey the right-hand rule, we can predict that the loop trajectory observed in figure 16 can be obtained equivalently by considering a negative magnetic field for the $\varphi = \pi/4$ direction of propagation. Recent papers [26, 42] have demonstrated that an electron moving in a graphene sheet bent into an arc of a circle behaves as if it was subjected to a pseudo-magnetic field that points in the opposite direction for each valley K and K′ of the graphene spectrum. This allows us to separate wavepackets in different valleys in a simple way [43]: we just need to consider a $\varphi = \pi/4$ incidence on a pseudo-magnetic step barrier, so that the Lorentz force would lead to a reflection of electrons in the K valley, whereas the electrons in K′ would penetrate and cross the pseudo-magnetic barrier, since the pseudo-magnetic field for this valley is negative, which leads to a loop-like trajectory as in figure 16.

4. Conclusions

We have presented a theoretical study of the time evolution of wavepackets in two types of systems: a 2DEG, where the electrons obey the Schrödinger equation, and a graphene layer, where they obey the massless Dirac equation for low energies. By comparing the trajectories obtained for these two cases to those of analogous classical particles, significant discrepancies

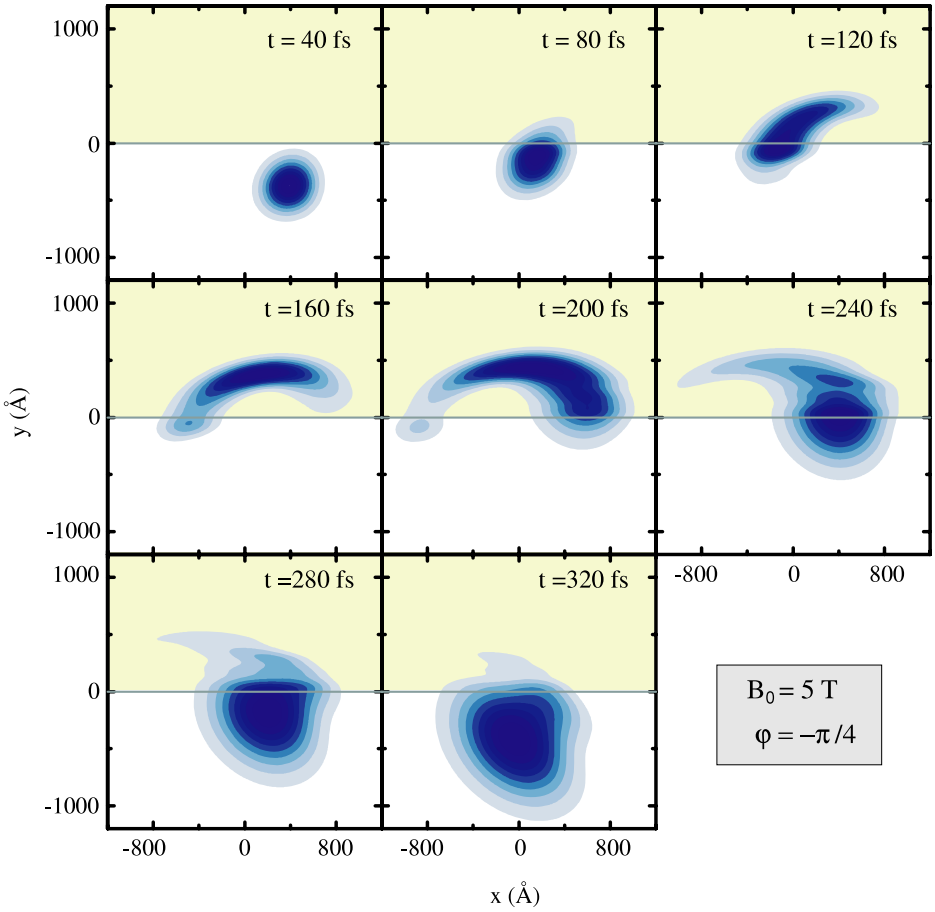

Figure 17. Contour plots of $|\Psi|^2$ for different time instants, considering the same parameters as in figure 16, for $B_0 = 5$ T. Darker (lighter) colours represent higher (lower) values of the probability density.

can be observed between the quantum and the classical cases for a number of examples. In the 2DEG case, this happens mostly due to the wave character of the particle. As we have a distribution of energies in the wavepacket, part of this packet can be transmitted over a potential barrier, even if the average energy of the packet is smaller than the barrier height. Conversely, even for wavepacket average energies larger than the barrier height, a low-energy tail of the wavefunction can still be reflected by the barrier.

In the case of Dirac fermions, we demonstrate the effect of Klein tunnelling using the propagation of a wavepacket through a potential step barrier. Indeed, we observe a very high transmission probability, which is shown to be a consequence of the transition from electron to hole states inside the barrier. We also demonstrated that the wavepacket distortions due to the admixture of electron and hole states are intensified for a tunnelled wavepacket with energy close to the barrier height.

Our results for non-zero mass in graphene suggest that the amplitude and the period of zitterbewegung can be enhanced by the presence of a mass-related potential, which can be experimentally obtained by means of a site-dependent potential induced by the substrate, and which also opens a gap in the graphene energy spectrum. A wavepacket which is expected to propagate only along the y axis is shifted in the x direction when it is reflected by a mass barrier, due to the zitterbewegung. This suggests a way to (indirectly) detect this effect experimentally, by comparing the initial and final trajectories of a packet reflected by a substrate-induced barrier potential.

In the presence of a magnetic field step barrier, the trajectories of both Schrödinger and Dirac particles exhibit circular profiles, as expected, due to the Lorentz force. On the other hand, the radii and position of these circles are not the same as those obtained for a classical particle, due to the wave character of the particles in the quantum case. The fact that the trajectories of wavepackets in graphene also obey the right-hand rule suggests an easy way to separate the packets in the K and K′ Dirac points of the graphene energy spectrum by using a strain-induced pseudo-magnetic field: as the strain induced a field pointing in opposite directions for each valley, the trajectories for wavepackets with slanted incidence at a pseudo-magnetic field barrier would naturally follow completely different directions, allowing a valley filtering, which is of relevance for future valleytronic devices.

Acknowledgments

Discussions with A Matulis are gratefully acknowledged. KR is beneficiary of a mobility grant from the Belgian

Federal Science Policy Office, co-funded by the European Commission and was supported in part by a grant of the Third World Academy of Sciences (ref. 09-188 RG/PHYS/AS-I). In addition, this work was financially supported by CNPq, under contract NanoBioEstruturas 555183/2005-0, PRONEX/FUNCAP, CAPES, the Bilateral programme between Flanders and Brazil, the joint project CNPq-FWO, the Belgian Science Policy (IAP) and the Flemish Science Foundation (FWO-Vl).

References

[1] Tsu R and Esaki L 1973 *Appl. Phys. Lett.* **22** 562
[2] Degani M H, Farias G A and Peeters F M 2005 *Phys. Rev.* B **72** 125408
[3] de Sousa J S, Freire J A K and Farias G A 2007 *Phys. Rev.* B **76** 155317
[4] Chaves A, Farias G A, Peeters F M and Szafran B 2009 *Phys. Rev.* B **80** 125331
[5] Maksimova G M, Demikhovskii V Ya and Frolova E V 2008 *Phys. Rev.* B **78** 235321
[6] Lherbier A, Biel B, Niquet Y-M and Roche S 2008 *Phys. Rev. Lett.* **100** 036803
[7] Novoselov K S, Geim A K, Morozov S V, Jiang D, Zhang Y, Dubonos S V, Grigorieva I V and Firsov A A 2004 *Science* **306** 666
[8] Castro Neto A H, Guinea F, Peres N M R, Novoselov K S and Geim A K 2009 *Rev. Mod. Phys.* **81** 109
[9] Thaller B 2004 Visualizing the kinematics of relativistic wavepackets, arXiv:quant-ph/0409079v1
[10] Demikhovskii V Ya, Maksimova G M, Perov A A and Frolova E V 2010 *Phys. Rev.* A **82** 052115
[11] Simicevic N 2008 Three-dimensional finite difference-time domain solution of Dirac equation, arXiv:0812.1807v1 [physics.comp-ph]
Simicevic N 2009 Finite difference-time domain solution of Dirac equation and the Klein paradox , arXiv:0901.3765v1 [quant-ph]
[12] Schrödinger E 1930 *Sitzungsber. Peuss. Akad. Wiss., Phys. Math. Kl.* **24** 418
See also Barut A O and Bracken A J 1981 *Phys. Rev.* D **23** 2454
[13] Krekova P, Su Q and Grobe R 2004 *Phys. Rev. Lett.* **93** 043004
[14] Ferrari F and Russo G 1990 *Phys. Rev.* B **42** 7454
[15] Gerritsma R, Kirchmair G, Zähringer F, Solano E, Blatt R and Roos C F 2010 *Nature* **463** 68
[16] Rusin T M and Zawadzki W 2009 *Phys. Rev.* B **80** 045416
[17] Rusin T M and Zawadzki W 2010 *Phys. Rev.* D **82** 125031
[18] Dombey N and Calogeracos A 1999 *Phys. Rep.* **315** 41
[19] Stander N, Huard B and Goldhaber-Gordon D 2009 *Phys. Rev. Lett.* **102** 026807
[20] Young A F and Kim P 2009 *Nature Phys.* **5** 222
[21] Matulis A and Peeters F M 2008 *Phys. Rev.* B **77** 115423
[22] Matulis A, Peeters F M and Vasilopoulos P 1994 *Phys. Rev. Lett.* **72** 1518
[23] De Martino A, Dell'Anna L and Egger R 2007 *Phys. Rev. Lett.* **98** 066802
[24] Masir M R, Vasilopoulos P, Matulis A and Peeters F M 2008 *Phys. Rev.* B **77** 235443
[25] Masir M R, Vasilopoulos P and Peeters F M 2010 *J. Phys.: Condens. Matter* **22** 465302
[26] Chaves A, Covaci L, Rakhimov Kh Yu, Farias G A and Peeters F M 2010 *Phys. Rev.* B **82** 205430
[27] Gaddam S, Bjelkevig C, Ge S, Fukutani K, Dowben P A and Kelber J A 2011 *J. Phys.: Condens. Matter* **23** 072204
[28] Zhou S Y, Gweon G-H, Fedorov A V, First P N, de Heer W A, Lee D-H, Guinea F, Castro Neto A H and Lanzara A 2007 *Nature Mater.* **6** 770
[29] Degani M H and Leburton J P 1991 *Phys. Rev.* B **44** 10901
[30] Suzuki M 1990 *Phys. Lett.* A **146** 319
[31] Watanabe N and Tsukada M 2000 *Phys. Rev.* E **62** 2914
[32] Pereira J M Jr, Peeters F M, Chaves A and Farias G A 2010 *Semicond. Sci. Technol.* **25** 033002
[33] Governale M and Ungarelli C 1998 *Phys. Rev.* B **58** 7816
[34] Peeters F M and Matulis A 1993 *Phys. Rev.* B **48** 15166
[35] Schnez S, Ensslin K, Sigrist M and Ihn T 2008 *Phys. Rev.* B **78** 195427
[36] Katsnelson M I, Novoselov K S and Geim A K 2006 *Nature Phys.* **2** 620
[37] Pereira J M Jr, Mlinar V, Peeters F M and Vasilopoulos P 2006 *Phys. Rev.* B **74** 045424
[38] Hartman T E 1962 *J. Appl. Phys.* **33** 3427
[39] Wu Z, Chang K, Liu J T, Li X J and Chan K S 2009 *J. Appl. Phys.* **105** 043702
[40] Sepkhanov R A, Medvedyeva M V and Beenakker C W J 2009 *Phys. Rev.* B **80** 245433
[41] Dragoman D and Dragoman M 2010 *J. Appl. Phys.* **107** 054306
[42] Low T and Guinea F 2010 *Nano Lett.* **10** 3551
[43] Wu Z, Zhai F, Peeters F M, Xu H Q and Chang K 2010 arXiv:1008.4858v3 [cond-mat.mes-hall]